

# IMPROVED MODELLING OF VORTICAL MIXING FOR THE SIMULATION OF EFFICIENT PROPULSION SYSTEMS

S. Saegeler\* , J. Lieser\*\* , Ch. Mundt\*

\*University of the German Federal Armed Forces Munich, \*\*Rolls-Royce Deutschland  
 sebastian.saegeler@unibw.de; jan.lieser@rolls-royce.com; christian.mundt@unibw.de

**Keywords:** hot jets, lobed mixer, turbulence, temperature correction

## Abstract

*More efficient and environmental friendly powerplants for air transportation are required. Therefore a deep understanding of all components of an aeroengine is necessary to fulfil the increasing requirements. One of these components is the exhaust system, which is the focus in this study.*

*The flow through the nozzle system with installed lobed forced mixer with scarfing is simulated using Favre-averaged Navier-Stokes solvers to study the mixing of the hot core and cold fan streams behind the mixer. Two turbulence models were used in this work. First, the well known  $k-\omega$ -SST turbulence model was applied. To capture high temperature effects, the  $k-\omega$ -SST model then was extended by a temperature correction method to improve the prediction of mixing in shear layers with large temperature gradients. Besides the commercial software Ansys Fluent, the open source code OpenFOAM was used.*

*The computational results of both turbulence models are presented in this paper and the performance calculations are compared to experimental data. While the original model underpredicts mixing in regions of hot and cold shear layers, the temperature corrected  $k-\omega$ -SST model shows better agreement with results from experiments.*

## 1 Introduction

Modern powerplants for aircraft have reached a highly advanced stage. Further improvements

concerning noise emission or fuel consumption are getting more and more challenging.

While a few decades ago, generation and evaluation of experimental data was the main part of the development process of an aircraft engine, today the use of modern simulation techniques is highly increasing. Despite of using modern high performance computers, the application of computational fluid dynamics (CFD) is limited and depends on the complexity of the problem. A remedy is to simplify the governing physical equations and find models to describe the physics. One approach is the usage of the Reynolds-Averaged Navier-Stokes equations (RANS). The RANS method time-averages the physical quantities (within time-scales such that fluctuating quantities are eliminated) and is a practical approach computing complex problems in an acceptable time. To compensate the loss of information through averaging, the influence of fluctuating quantities has to be modeled. A wide spread method is therefore two-equation turbulence models to describe the turbulent kinetic energy that mimics velocity fluctuations.

The mixing efficiency of the hot core and the cold bypass stream in a mixed nozzle system plays an important role concerning performance and noise emission. To improve mixing in mid-bypass ratio mixed jet engines, lobed forced mixers are installed. These mixers generate a complex system of vortices in their wake and lead to a more homogeneous distribution of temperature at the nozzle exit. An improved mixing rate can increase thrust and also reduce noise

emission [1]. To further push the development of more sophisticated powerplants, reliable simulation tools are necessary. In general it can be said, that the standard RANS models underpredict the mixing rates of jets. This problem increases for hot jets and lack the ability to properly predict the flow field as shown by [2]-[5]. One reason is, that the mentioned very popular two-equation turbulence models only aim to improve the prediction of the flow field regarding velocity fluctuations. High temperature effects, such as density and temperature fluctuations, are not taken into account. In the Favre-averaged compressible Navier-Stokes equations (FANS), physical quantities are also averaged by density and therefore density fluctuations are eliminated.

Several authors [6]-[8] have tried to improve the flow field prediction for high speed jets. Also with respect to high temperature effects. They either tried to change the coefficients or the closing terms of the turbulence equations. However, such extensive modifications always change the characteristics of the equations and may cause a deficiency in the flow prediction accuracy for other problems. Abdol-Hamid et al. [9] however have chosen a more general approach. Seiner et al. [4] and Thomas et al. [5] showed in their works, that high total temperature gradients lead to faster mixing and spreading of jet flow. Based on this empirical knowledge, an extension to the well known k- $\epsilon$  turbulence model [10] has been developed. The idea behind the new model is to increase eddy viscosity in the vicinity of large total temperature gradients to force mixing. In regions, where the total temperature are getting small, as in boundary layer flows (adiabatic walls assumed), the turbulence model returns to its original form without correction.

The superior behavior of Menter's k- $\omega$ -SST turbulence model [11], near walls and in free stream regions, it is a favorable model for a wide range of flow applications. Motivated by this aspects, and the facts, that the k- $\omega$ -SST and the k- $\epsilon$  model only differ in regions close to walls, in this study Abdol-Hamid's temperature correction method has been combined with Menter's SST model.

Two different flow solvers have been used. While a mesh sensitivity study was conducted with the commercial software Ansys Fluent, the open source code OpenFOAM was used for all other simulations.

## 2 Turbulence Model and Temperature Correction

### 2.1 k- $\omega$ -SST Turbulence Model

The k- $\omega$ -SST turbulence model of Menter is a two-layer model. It employs the k- $\omega$  model of Wilcox [12] in the inner region of the boundary layer and switches to the k- $\epsilon$  [10] model in the outer region of the boundary layer. The model combines the advantages of both turbulence models. While the k- $\omega$  shows better behavior in boundary layer flows, the k- $\epsilon$  model has advantages in free stream flows and mixing regions. The k- $\epsilon$  model is transformed into the k- $\omega$  form to provide a second set of k- $\omega$  equations with a blending function used to transition between the two sets of equations. Details of the complete k- $\omega$ -SST turbulence model are provided in [11],[13],[14]. For the sake of simplicity, only the outer part of the model shall be considered here. The k- $\omega$  set of equations is as follows:

$$\frac{D(\rho k)}{Dt} = \tau_{ij} \frac{\partial u_i}{\partial x_j} - \rho \beta^* \omega k (1 + Ma_t^2) + \frac{\partial}{\partial x_i} \left[ (\mu_t + \sigma_{k2} \mu_t) \frac{\partial k}{\partial x_i} \right], \quad (1)$$

$$\frac{D(\rho \omega)}{Dt} = \gamma_2 \frac{\rho}{\mu_t} \tau_{ij} \frac{\partial u_i}{\partial x_j} - \rho \beta_2 \omega^2 + \rho \beta^* \omega^2 Ma_t^2 + \frac{\partial}{\partial x_i} \left[ (\mu_t + \sigma_{\omega 2} \mu_t) \frac{\partial \omega}{\partial x_i} \right] + 2\rho \sigma_{\omega 2} \frac{1}{\omega} \frac{\partial k}{\partial x_i} \frac{\partial \omega}{\partial x_i}. \quad (2)$$

The model constants are  $\beta_2 = 0.0828$ ,  $\gamma_2 = 0.44$ ,  $\beta^* = 0.09$ ,  $\sigma_{k2} = 1.0$  and  $\sigma_{\omega 2} = 0.856$ . The turbulent viscosity is calculated as

$$\mu_t = \frac{\rho a_1 k}{\max(a_1 \omega, SF_2)}. \quad (3)$$

While  $a_1 = 0.31$ ,  $S$  is the invariant measure of the strain rate and  $F_2$  is a blending function. Away from walls  $F_2$  tends to zero, and thus the eddy viscosity reduces to  $\mu_t = \rho k / \omega$  in the outer region. Compared to the original k- $\omega$ -SST model, here the model has been further extended with the compressibility correction of Sarkar [15], which introduces the turbulent Mach number  $Ma_t$ . This correction has also been used in [9] with the k- $\varepsilon$  model. The compressibility correction was applied according to [16].

## 2.2 Temperature Correction

In [9], the temperature correction model was built upon the k- $\varepsilon$  turbulence model. Abdol-Hamid et al. noticed that standard turbulence models fail to capture the increase in the shear layer growth rate due to temperature effects. They devised a correction, that deals with these effects. The model was calibrated to the supersonic jet experiment of Seiner et al. [4]. In this work, the eddy viscosity was multiplied by a factor  $C_T$  that depends on local total temperature gradients. The original formulation of  $C_T$  is defined as

$$C_T = \left[ 1 + \frac{T_g^3}{0.041 + f(Ma_t)} \right], \quad (4)$$

where  $T_g$  is the normalized total temperature gradient:

$$T_g = \frac{|\nabla T_t| k^{3/2}}{T_t \varepsilon}. \quad (5)$$

$f(Ma_t)$  is a compressibility function depending on the turbulent Mach number  $Ma_t$ , similar to the correction of Sarkar.

Now expression (5) has to be transformed into k- $\omega$  form. This can be done with the following relation:

$$\varepsilon = \beta^* k \omega. \quad (6)$$

The transformed normalized total temperature gradient is then

$$T_g = \frac{|\nabla T_t| k^{1/2}}{T_t \beta^* \omega}, \quad (7)$$

and the new eddy viscosity for the k- $\omega$ -SST model is

$$\mu_t = \frac{C_T \rho a_1 k}{\max(a_1 \omega, S F_2)}. \quad (8)$$

However, the new  $\mu_t$  (8) containing the factor  $C_T$  can not just be used in conjunction with equation (2). In order to be consistent with the effect of the correction within the k- $\varepsilon$  model, equation (2) has to be changed:

- The first term on the right side of equation (2) has to be multiplied by  $C_T$ . This can be seen when doing the exact transformation from the  $\varepsilon$ - to the  $\omega$ -equation with respect to the new eddy viscosity.
- The last term in the  $\omega$ -equation has to be multiplied by  $C_T$ . In the exact transformation of the  $\varepsilon$ - to the  $\omega$ -equation (see in [17]), the kinematic viscosity  $\nu_t$  appears in the cross-diffusion term. Obviously the term  $k/\nu_t$  has been replaced by  $1/\omega$ . Thus, there is a hidden turbulent viscosity and the factor  $C_T$  has to be applied here as well.

Now the new  $\omega$ -equation with temperature correction for the SST model reads as

$$\begin{aligned} \frac{D(\rho\omega)}{Dt} = & \gamma_2 \frac{\rho}{\mu_t} \tau_{ij} \frac{\partial u_i}{\partial x_j} C_T - \rho \beta_2 \omega^2 + \rho \beta^* \omega^2 Ma_t^2 \\ & + \frac{\partial}{\partial x_i} \left[ (\mu_l + \sigma_{\omega 2} \mu_t) \frac{\partial \omega}{\partial x_i} \right] \\ & + 2\rho \sigma_{\omega 2} \frac{C_T}{\omega} \frac{\partial k}{\partial x_i} \frac{\partial \omega}{\partial x_i}. \end{aligned} \quad (9)$$

It should be pointed out here again, that in regions where no large total temperature gradients occur, for instance in boundary layer flows with adiabatic walls etc.,  $C_T$  tends to unity and so the temperature corrected turbulence model turns back into its original form with no correction.

A comparison between the temperature correction applied to the k- $\omega$ -SST model and the k- $\varepsilon$  model, which was used in the original paper by Abdol-Hamid, can be found in [18].

### 3 Numerical Setup and Configurations

#### 3.1 Computational Model

##### 3.1.1 Mesh

The geometry of the nozzle and the lobed mixer with scarfing was provided by Rolls-Royce Deutschland. The geometry was scaled by a factor of 0.18 to be coincident with the scale used in experiments. For meshing, a  $45^\circ$  slice of the whole nozzle system was used and has been meshed fully structured. The two boundaries on the left and right side of the  $45^\circ$  slices were defined as symmetry planes. Figure 1 shows the geometry and symmetry plane with mesh lines. The main focus in this work was on the flow field

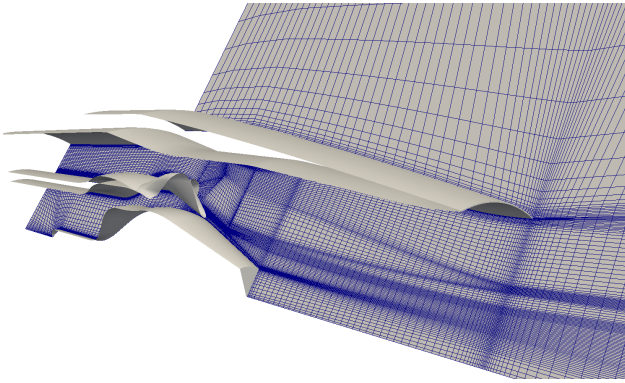


**Fig. 1** Geometry of the  $45^\circ$  nozzle system with lobed mixer and symmetry plane with mesh lines.

right behind the mixer, as well as the examination of performance coefficients. Therefore, to keep the numerical effort low, the size of the domain was kept small. The outlet downstream is located 1.5 nozzle diameters from the nozzle exit. The distance from the symmetry axis to the upper boundary of the domain is 2.5 diameters. Figure 2 shows the full domain. To further save mesh cells, the mesh was designed to be able to run the  $k-\omega$ -SST model with wall functions. The first grid cell off the wall was created such that the value of  $y^+$  is about 30. Although the mesh was designed very carefully to achieve this value, it is not possible to reach  $y^+ = 30$  everywhere on the walls and for all calculations performed, because only one mesh was created for all simulations

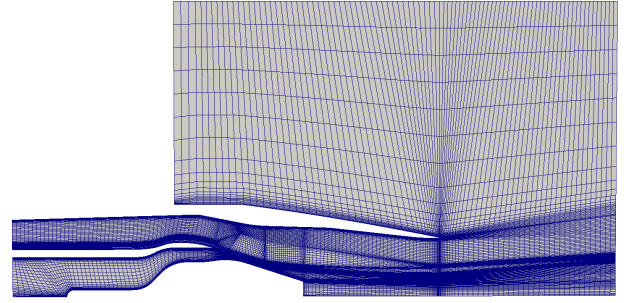


**Fig. 2** Numerical domain.

with different boundary conditions. Further, the complexity of the flow and the geometry makes it impossible to reach a homogeneous distribution of  $y^+ = 30$  everywhere. The averaged values achieved for  $y^+$  in all calculations are within a range of  $31.9 < y^+ < 64.6$ .

The overall size of the mesh displayed in figure 2 is about 1.25 million cells.

##### 3.1.2 Solver

While the commercial software Ansys Fluent was used for the mesh sensitivity study, all other simulations were conducted with the open source code OpenFOAM. The Fluent calculations were run with a coupled pressure based algorithm. The simulations in OpenFOAM were performed with a density based Riemann solver [19] that has been further combined with a preconditioner [20].

Air was used as fluid and treated as an ideal gas. For the OpenFOAM calculations a constant specific heat capacity of  $c_p = 1007$  J/kgK was used.

#### 3.2 Configurations

Several operating conditions of the nozzle flow were simulated. The following quantities have been determined to define the boundary conditions:

- CNPR (cold nozzle pressure ratio):  $p_{t, fan} / p_\infty$
- PS (pressure split):  $p_{t, fan} / p_{t, core}$

- TR (temperature ratio):  $T_{t,core}/T_{t,fan}$

Total temperatures at the inlets of the fan and the farfield have been always set to 288.15 K. The ambient pressure has a value of  $p_\infty = 101148$  Pa. Now all other total quantities at the fan and core inlets can be calculated using the values in table 1. The co-flow in the farfield has been set such that the Mach number is  $Ma_\infty = 0.05$  ( $p_{t,\infty} = 101325$  Pa).

CNPR	PS	TR
1.6	1.1	1.0
		1.5
		2.0
		2.4
2.6	1.1	1.0
		1.5
		2.0
		2.4
		2.55

**Table 1** Simulated operating conditions of the nozzle flow.

#### 4 Experimental Setup

In order to gather data for improved modelling of future mixed nozzle engines for application at business jets a dedicated test was performed in the Channel 11 static thrust measurement rig at ASE FluidDyne Aerotest Laboratory in Plymouth, Minnesota. The aim of the test was to systematically investigate nozzle charging parameter changes. This enables to determine nozzle characteristics independent of the engine matching. The focus in the presented work is the thrust increase achieved by mixing. Therefore the nozzle integral values such as velocity coefficient and discharge coefficients were determined for a variation of temperature ratios up to the limit of the facility (see chapter 5). Channel 11 is a dual flow static thrust stand. Nozzle thrust is determined from force measurements with a strain gage force balance. The mass flow through the cold and hot side of the mixed nozzle is metered by ASME nozzles. The facility is supplied by

pressurized air from a dry air storage system. To heat up the core flow air can be passed through a regenerative storage heater, mixed with the cold air to achieve the desired temperature. As mentioned in the previous chapter, the model is 18% scaled from an engine design with a max take of thrust of around 13.000 lbf ( $\approx 57827$  N) and is displayed in figure 3. The model is equipped with total pressure rakes, wall statics and temperature rakes to determine the nozzle charging conditions. The model is equipped with a hot and

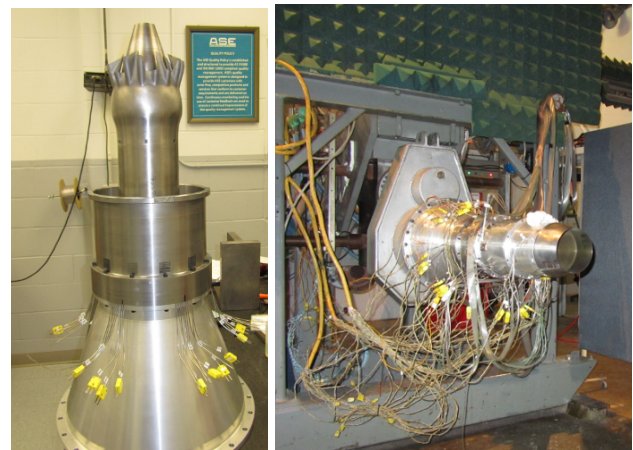


**Fig. 3** Left: Forced mixer and bullet (bypass and fan nozzle disassembled). Right: Mixed exhaust model installed at the static thrust rig.

cold spacer to account for thermal expansion at a temperature ratio of 2.6. For lower temperatures the hot spacer is not changed which may lead to some inaccuracies at a maximum for the comparison of cold and lowest temperature measurement. In addition the charging temperatures are determined by the rake measurement in hot cases and by a Joule Thompson correction from the facility measurements in case of cold flow. An extrapolation of the hot cases to cold cases is therefore at risk.

#### 5 Performance Analysis

To evaluate the results with respect to performance, some parameters had to be determined. The velocity coefficient  $C_V$  as well as the discharge coefficient  $C_D$  were chosen to quantify and study the performance of the nozzle system.

A definition for the velocity coefficient can be found in reference [21]:

$$C_V = \frac{u_{exit}}{u_{exit,id.}}, \quad (10)$$

and is the ratio of velocity at the nozzle exit and the ideal exit velocity. Here the velocity coefficient is calculated by evaluating the gross thrust:

$$C_V = \frac{F_{G,x}}{\dot{m} u_{id}}. \quad (11)$$

$\dot{m}$  is the measured mass flow through the nozzle,  $u_{id}$  is the ideal exit velocity and  $F_{G,x}$  is the evaluated gross thrust in x-direction. The ideal velocity that can be achieved at the nozzle exit is calculated by the formula of de Saint-Venant and Wantzel [22] and yields:

$$u_{id} = \sqrt{\frac{2\kappa T_t R}{\kappa - 1} \left( 1 - \left( \frac{p_t}{p_\infty} \right)^{\frac{1-\kappa}{\kappa}} \right)}. \quad (12)$$

To solve for the gross thrust  $F_{G,x}$ , the momentum balance in x-direction around the control volume (see figure 4) is calculated:

$$F_{G,x} = \int_{A_{fan}} \rho u^2 dA + \int_{A_{core}} \rho u^2 dA + \int_{A_{fan}} (p - p_\infty) dA + \int_{A_{core}} (p - p_\infty) dA + \int_{A_{walls}} \sigma_x dA, \quad (13)$$

where  $\sigma_x$  is the surface force density in x-direction, integrated over the area of all inner walls  $A_{walls}$  of the nozzle. For a mixed nozzle

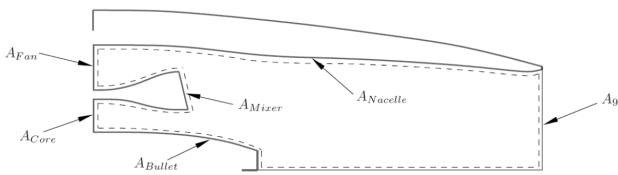


**Fig. 4** Schematic view of the control volume.

system the denominator in (11) is split into a portion of fan and core [21]. It is finally defined as

$$C_V = \frac{F_{G,x}}{(\dot{m} u_{id})_{fan} + (\dot{m} u_{id})_{core}}. \quad (14)$$

The discharge coefficient  $C_D$  can be found in [21] and compares the ideal mass flow through the nozzle with the mass flux actually reached. For a single stream nozzle, this is

$$C_D = \frac{\dot{m}}{\dot{m}_{id}} = \frac{1}{A_{throat}} \frac{\dot{m} \frac{\sqrt{T_t}}{p_t}}{Q_{ideal}}. \quad (15)$$

$Q$  is the reduced mass flow or  $Q$ -function and is given by

$$Q = \frac{\dot{m} \frac{\sqrt{T_t}}{p_t}}{A_{throat}}. \quad (16)$$

The ideal  $Q$  is defined as

$$Q_{ideal} = \frac{\dot{m}_{ideal} \frac{\sqrt{T_t}}{p_t}}{A_{throat}} = \left( \frac{p}{p_t} \right)^{\frac{1}{\kappa}} \sqrt{\frac{2\kappa}{R(\kappa - 1)} \left( 1 - \left( \frac{p}{p_t} \right)^{\frac{\kappa-1}{\kappa}} \right)}, \quad (17)$$

$$\text{with } \begin{cases} p_t/p < p_t/p^*, & p = p_\infty \\ p_t/p > p_t/p^*, & p = p^* \end{cases},$$

where  $p_t/p^*$  is the critical pressure ratio, and  $\kappa$  the ratio of specific heat capacities. This definition of  $C_D$  is applicable for a single stream exiting the nozzle. From [21] it can be seen that the discharge coefficient can also be expressed as the ratio of the effective area to geometric area. The effective area ( $A_{eff} = C_D \cdot A$ ) is computed according to the definition in equation (15) of the discharge coefficient based on measured/computed mass flows. In case of mixed streams exiting the nozzle it is a common practice to calculate the discharge coefficient as a sum of effective areas of both streams over the area of the throat:

$$C_D = \frac{\sum A_{eff}}{A_{throat}} = \frac{1}{A_{throat}} \left[ \left( \frac{\dot{m} \frac{\sqrt{T_t}}{p_t}}{Q_{ideal}} \right)_{fan} + \left( \frac{\dot{m} \frac{\sqrt{T_t}}{p_t}}{Q_{ideal}} \right)_{core} \right]. \quad (18)$$

6 Results

6.1 Mesh Sensitivity

A mesh sensitivity study was conducted to determine the influence of grid resolution on the accuracy of the solution. Three different grids were created. Starting point was a mesh with 1.25 million cells in the domain. Then the size of the mesh has been increased twice by expanding the number of nodes by a factor of 1.5 in each spatial direction. The resulting grids have the size of 4.3m and 15m cells. To study the influence of the mesh, the simulations were run on all three grids for several boundary conditions: CNPR=1.6, 2.6; PS=1.1; TR=1.0, 2.4. For easier comparison of the runs with different flow conditions the following nomenclature is introduced to describe the cases: <CNPR>-<PS>-<TR>. For instance 2.6-1.1-2.4 means that the case was run with CNPR=2.6, PS=1.1 and TR=2.4. Figure 5 shows the dependency of  $C_D$  and  $C_V$  over the mesh resolution. On the abscissa, one over the number of mesh cells is plotted. It can be seen, that from the coarser mesh to the finest, the coefficients are increasing. Table 2 shows the increase of  $C_D$  and  $C_V$  compared to the coarsest mesh for the different operating conditions in percentage. For both cases of TR=1.6 and 2.4, the highest difference to the coarsest mesh is achieved for CNPR=1.6. The highest displacement here is a difference of 0.18% for  $C_D$  and 0.14% for  $C_V$ . A higher CNPR obviously does not lead to such big differences, the curves in fig. 5 run steeper for CNPR=1.6. It is also interesting to see, that for the same CNPR, either 1.6 or 2.6, a better resolution of the temperature field and thus a better capturing of sharp temperature gradients does not play such an important role. Comparing  $\Delta C_D$  and  $\Delta C_V$ , it seems that the discharge coefficient is a bit more sensitive to the grid resolution.

6.2 Effect of Temperature Correction

The k- $\omega$ -SST turbulence model, with and without temperature correction, was applied on the set of operating conditions from table 2. One goal was to study the flow field in the vicinity of the mixer

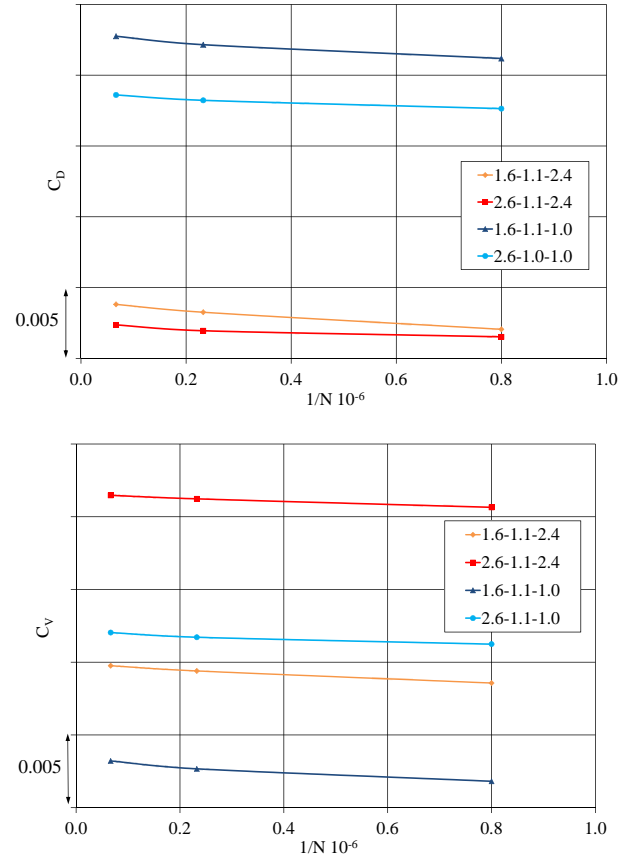


Fig. 5 Dependency of  $C_D$  and  $C_V$  on grid size.

and see how it changes due to the application of temperature correction. Also, the influence of temperature correction on the performance parameters has been studied, which is part of the next section. As the calculations presented here were conducted with OpenFOAM, where only a local time stepping scheme is available for con-

# Cells	$\Delta C_D$ %	$\Delta C_V$ %	CNPR	TR
4.3 m.	0.13	0.08	1.6	1.0
15.0 m.	0.18	0.12		
4.3 m.	0.10	0.09	1.6	2.4
15.0 m.	0.16	0.14		
4.3 m.	0.05	0.06	2.6	1.0
15.0 m.	0.09	0.08		
4.3 m.	0.06	0.05	2.6	2.4
15.0 m.	0.10	0.08		

Table 2 Changes of  $C_D$  and  $C_V$  compared to the coarsest mesh with 1.25 m. cells. PS=1.1.

vergence acceleration, the mesh containing 1.25 m. cells was used for simulation.

In figure 6 a longitudinal cut through the domain with distribution of the total temperature is depicted for case 1.6-1.1-2.4. The upper part shows the solution of the standard  $k\text{-}\omega\text{-SST}$  Model, and the lower one the temperature correction is applied. It can be seen that the solution with temperature correction on shows a slightly more diffusive total temperature distribution profile. This is even more obvious if regarding the contour plots at different  $x/D$ -stations in figure 7 ( $x$ -coordinate over nozzle exit diameter), where  $x/D=0.0$  is located at the nozzle exit. The diffusion of the total temperature also effects other quantities in the flow. So the maximum velocity reached in the domain always decreases in conjunction with temperature correction. For instance, in the case of 1.6-1.1-2.4, the maximum velocity magnitude drops from 368 m/s to 360 m/s, probably because of viscous effects. The top

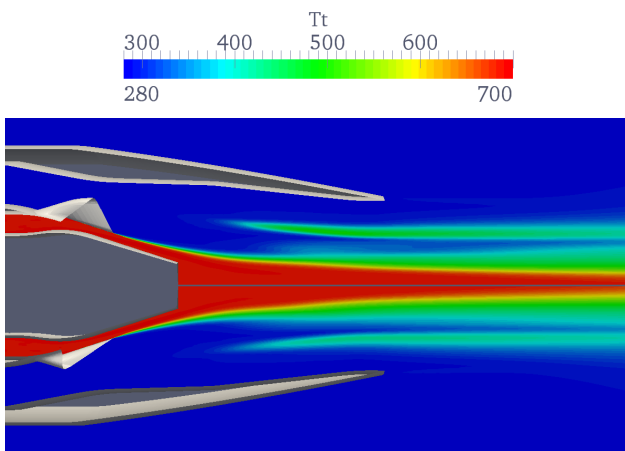


**Fig. 6** Section planes of total temperature profiles of case 1.6-1.1-2.4. Upper:  $k\text{-}\omega\text{-SST}$ . Lower:  $k\text{-}\omega\text{-SST}$  with temperature correction.

pictures show the total temperature contours right after the mixer exit. The change from cold to hot fluid is sharper than for the standard  $k\text{-}\omega\text{-SST}$  solution. At  $x/D=-0.7$  which is about the half way from mixer exit to nozzle exit, it can be seen that the high temperature peaks in the vortices have clearly decreased compared to the standard SST model. This trend continues in the following pic-

tures and can be seen especially in a shortening of the potential core.

In figure 8 the contours of the turbulent kinetic energy of both turbulence models are shown. Again, the upper part is without temperature correction, in the lower picture correction is on. The  $k\text{-}\omega\text{-SST}$  turbulence model with temperature correction produces more turbulent kinetic energy right behind the lobed mixer. It is interesting to see that the increased mixing of the hot and cold streams close to the mixer exit then leads to a lower production of turbulent kinetic energy when the jet is exiting the nozzle. The stronger spreading of the wake of the mixer probably leads to a decrease of the local velocity gradients and thus to a lower production of turbulence further downstream. In figure 9 contours of  $k$  are plotted at several  $x/D$ -stations.

### 6.3 Comparison of CFD and Experiments

To validate the computational data, performance parameters from experiments are available. The experimental and numerical results for  $C_D$  and  $C_V$  are depicted in figure 10. As it can be seen, the discharge coefficient is decreasing for rising temperature ratios. This is mainly because of a lower density in the core flow due to higher temperatures. The velocity coefficient on the contrary increases for higher TR. This is due to increasing losses for higher temperatures and temperature ratios. Here, the benefits of effective mixing of hot and cold streams become obvious. As already mentioned in the introduction, a well designed mixer can increase thrust. The definition of  $C_V$  in (14) is the ratio of the actually reached gross thrust over the thrust achieved with ideally but separately expanded core and fan streams. For higher temperature ratios, the benefit of mixing increases and thus  $C_V$  is raising. Comparing the solution of the numerical data, the turbulence model with temperature correction leads to a further decrease of  $C_D$  for higher TR. The effect of temperature correction on  $C_V$  is vice versa and the curves run steeper. Also a certain off-set for most of the curves can be seen compared to experiments. While  $C_D$  from simulation is always

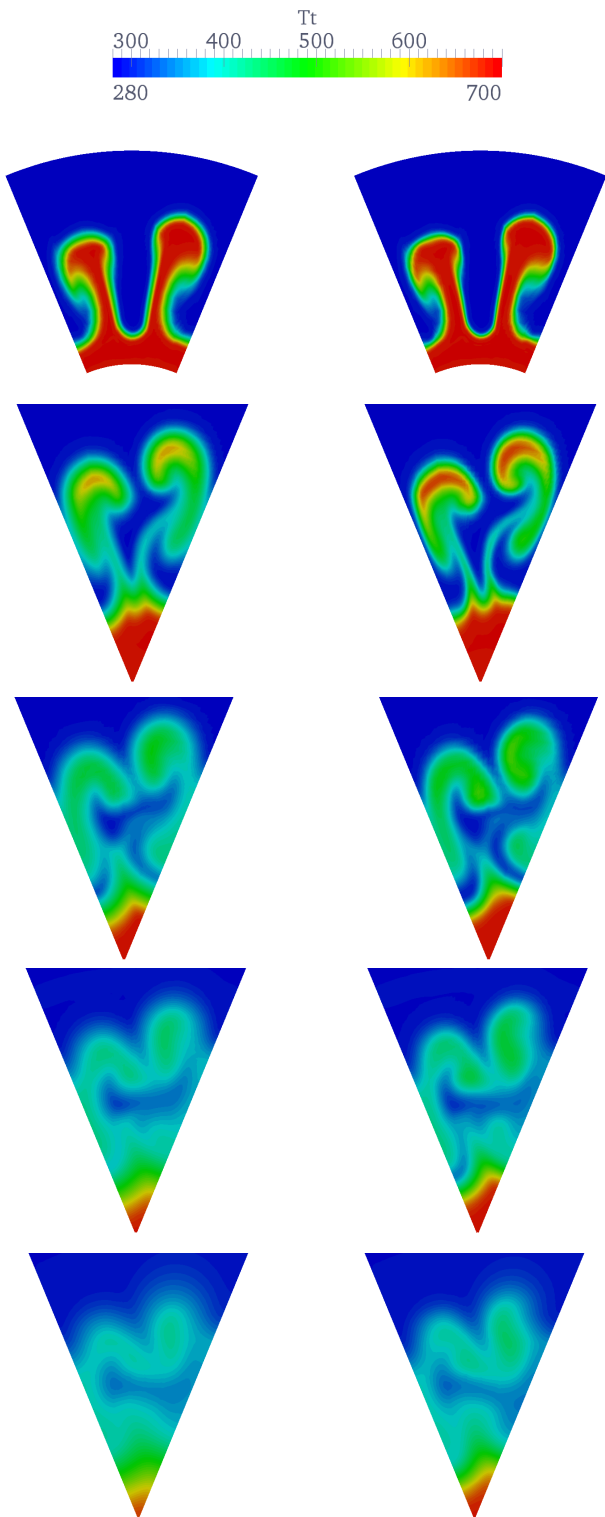


**Fig. 7** Section planes of total temperature profiles of case 1.6-1.1-2.4. Right:  $k-\omega$ -SST. Left:  $k-\omega$ -SST with temperature correction.  $x/D$ -stations from top to bottom: -1.4, -0.7, 0.0, 0.7, 1.4.

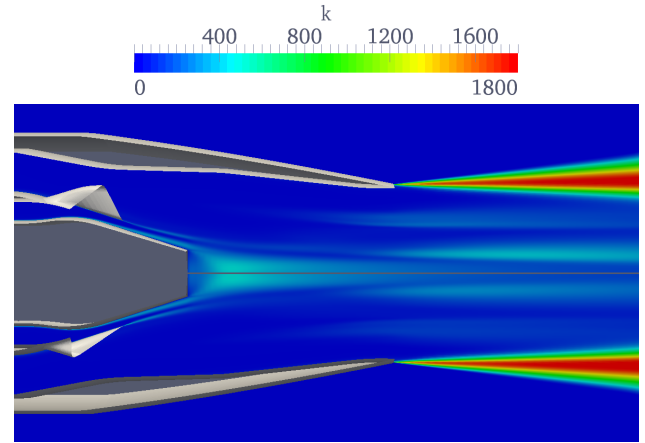


**Fig. 8** Section planes of turbulent kinetic energy of case 1.6-1.1-2.4. Upper:  $k-\omega$ -SST. Lower:  $k-\omega$ -SST with temperature correction.

predicted too low,  $C_V$  for  $CNPR=1.6$  is below experimental data and for  $CNPR=2.6$  the curves seem to fit better. This discrepancy might be due to several reasons. First, as mentioned in chapter 4, the model is equipped with a hot and cold spacer to account for thermal expansion at  $TR$  2.6. For lower temperatures, the hot spacer is not changed. Further, inaccuracies might be introduced because charging temperatures are determined by the rake measurement in hot cases and by a Joule Thompson correction from the facility measurements in case of cold flow. Second, for evaluating the performance parameters, in CFD the total values at the domain bounds are used. In experiments, the momentum-averaged values at the charging planes, right before mixer entry, have been used. Third, the resolution of the mesh used for simulations has been shown to be sensitive to the solution and a finer mesh would lead to higher  $C_V$  and  $C_D$ . Also, there might always be an uncertainty due to numerical schemes used.

A better comparison of numerical and experimental data may therefore give the relative changes of  $C_D$  and  $C_V$  over the temperature ratio. In figure 11  $\Delta C_D$ , and in figure 12  $\Delta C_V$  are plotted (experimental data are only displayed for  $TR \geq 1.5$ ). The most obvious deficiency between CFD and experiments again is the off-set of the curves. As mentioned, this might be due to the

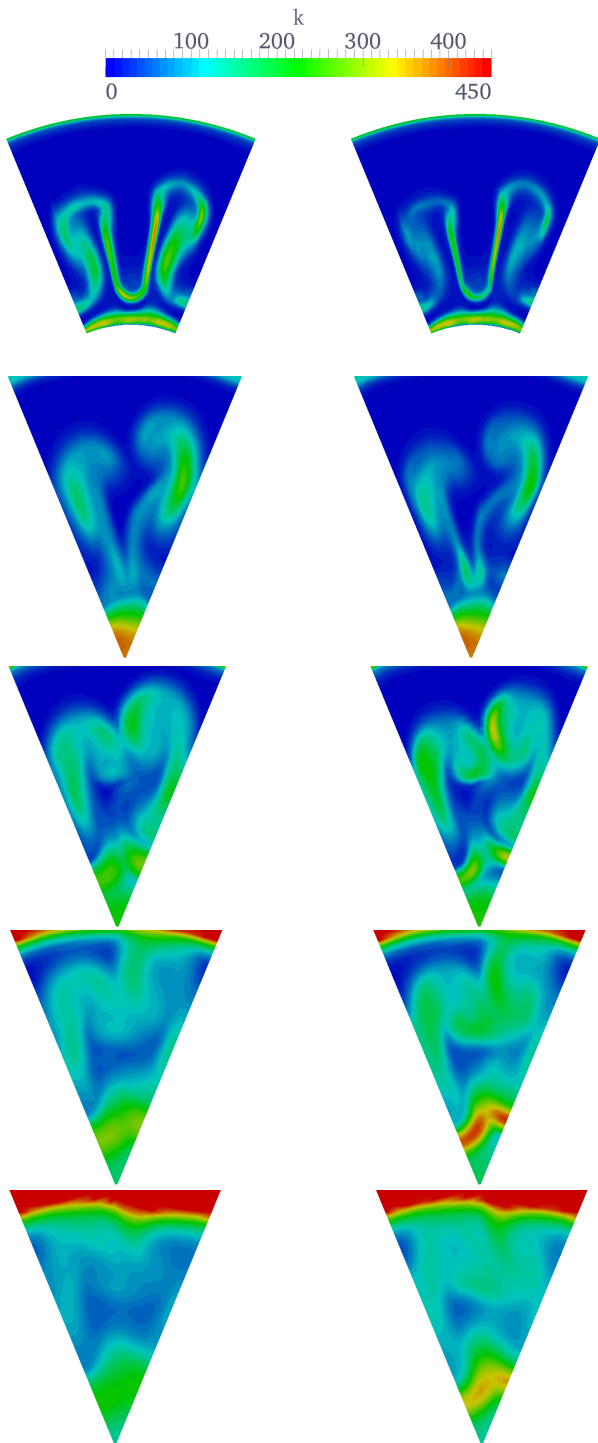


**Fig. 9** Section planes of turbulent kinetic energy profiles of case 1.6-1.1-2.4. Right:  $k-\omega$ -SST. Left:  $k-\omega$ -SST with temperature correction.  $x/D$ -stations from top to bottom: -1.4, -0.7, 0.0, 0.7, 1.4.

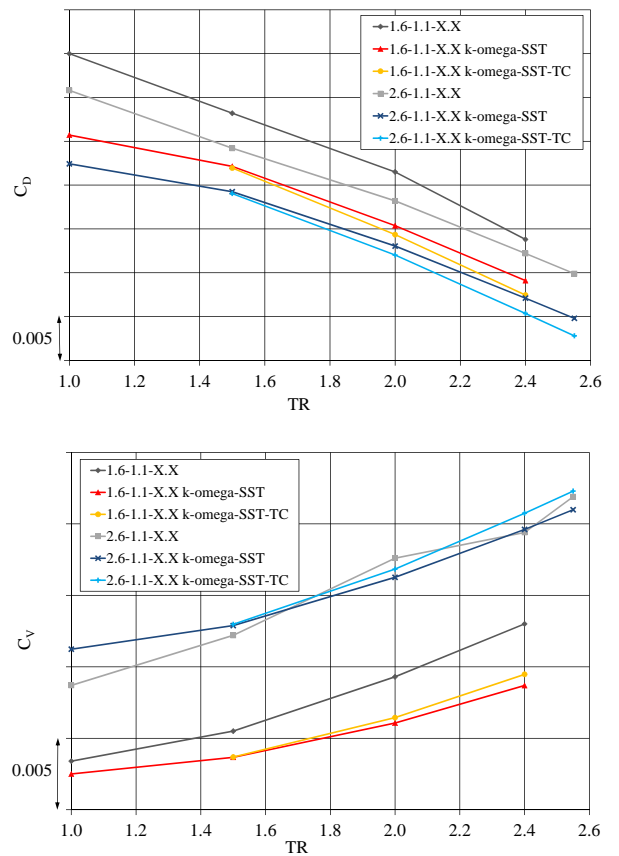


**Fig. 10** Curves of  $C_D$  and  $C_Y$  over  $TR$ . Experimental and numerical data.

experimental setup and the gain of charging temperatures that cause the deficiency in case of cold flow. Thus, for higher TR close to 2.6, the distribution of the curves of experiments an CFD should fit best, disregarding the off-set. It is notable, that for higher TR, the inclination of experimental and CFD curves are very close, even though temperature correction leads to steeper curves. For CNPR=2.6 the delta of the discharge coefficient is even steeper than experimental results, while the regular k- $\omega$ -SST model seems to agree better in this case. Results for  $\Delta C_V$  in figure 12 show similar behavior and an off-set to experiments can be seen. The agreement with experimental data is better for higher TR. Especially the k- $\omega$ -SST model with temperature correction predicts the inclination of  $\Delta C_V$  best.

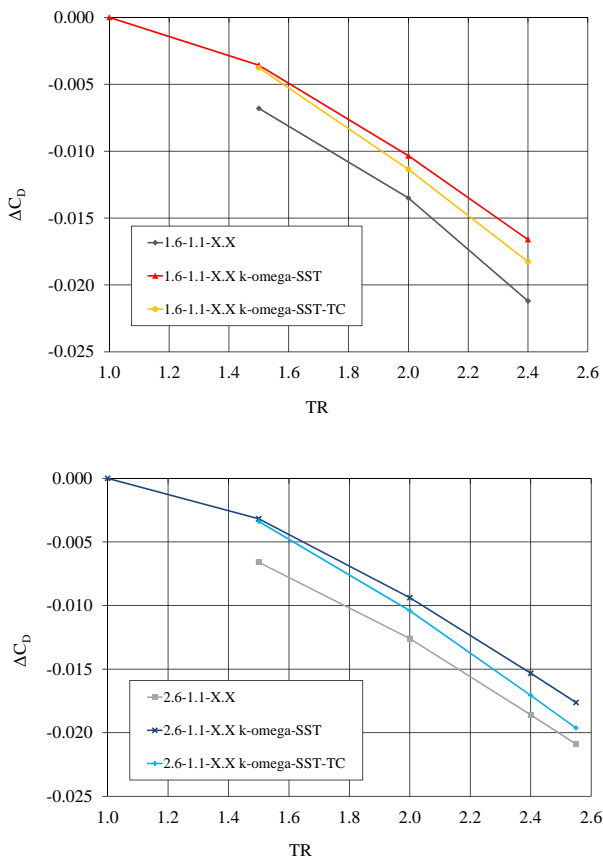


Fig. 11 Curves of  $\Delta C_D$  over TR. Experimental and numerical data.

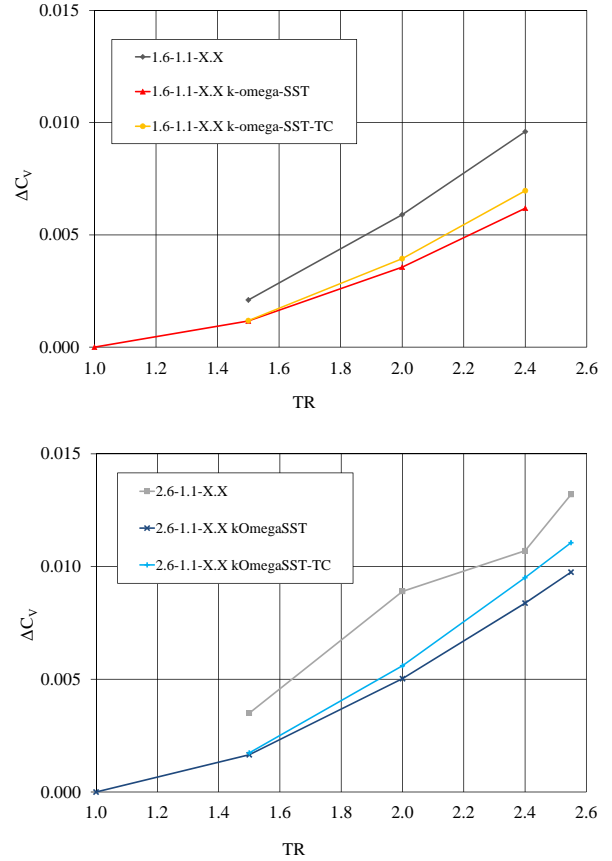


Fig. 12 Curves of  $\Delta C_V$  over TR. Experimental and numerical data.

### 7 Concluding Remarks

The objective of this work was to study the influence of two turbulence models on complex 3D mixing of hot and cold streams in the wake of a scarfed lobed mixer and the impact of the mesh on the solution. For this purpose, the k- $\omega$ -SST turbulence model with and without temperature correction has been applied. The correction was designed to account for increased mixing in flows with large temperature fluctuations and originally used with the k- $\epsilon$  model. It has been shown, that the temperature correction model leads to higher mixing in the wake of the lobed mixer. The higher production of turbulent kinetic energy right after the mixer exit is followed by a lower production of k compared to the standard k- $\omega$ -SST model. The increased mixing also impacts the performance parameters of the nozzle system. The discharge coefficient

further decreases for higher total temperature ratios with the temperature correction model. In case of 2.6-1.1-X.X the curve has even more inclination than experimental results. The velocity coefficient calculated with the temperature correction model increases for higher TR and thus comes closer to experimental data. However all curves show a certain off-set to the experimental data, which might have several reasons explained above. In general, the relative distribution of the curves from experiments and CFD are in good agreement.

Further, the grid sensitivity study has shown, that the solution for the performance parameters is depending on the number of cells. For a finer mesh, higher discharge and velocity coefficients are achieved.

## **8 Acknowledement**

This work is part of the OPTITHECK project, led by Rolls-Royce Deutschland, which is funded by the German Luftfahrtforschungsprogramm.

## **Copyright Statement**

The authors confirm that they, and/or their company or organization, hold copyright on all of the original material included in this paper. The authors also confirm that they have obtained permission, from the copyright holder of any third party material included in this paper, to publish it as part of their paper. The authors confirm that they give permission, or have obtained permission from the copyright holder of this paper, for the publication and distribution of this paper as part of the ICAS2012 proceedings or as individual off-prints from the proceedings.

References

- [1] Wegener M, Lieser J and Mundt Ch. Lärm- und leistungsoptimierter Strahlmischer. *DGLR Jahrestagung Berlin*, DGLR-JT99-82, 1999.
- [2] Koch L D and Bridges J. Flow field comparisons from three navier-stokes solvers for an axisymmetric separate flow jet. *40th Aerospace Science Meeting and Exhibit*, AIAA Paper No. 2002-0672, 2002.
- [3] Engblom W A, Khavaran A and Bridges J. Numerical prediction of chevron nozzle noise reduction using WIND-MGBK methodology. *10th AIAA/CEAS Aeroacoustics Conference*, DGLR/AIAA, AIAA Paper No. 2001-2979, 2001.
- [4] Seiner J M, Ponton M K, Jansen B J and Lagen T N. The effects of temperature on supersonic jet noise emission. *14th Aeroacoustics Conference*, DGLR/AIAA, AIAA Paper No. 92-02-046, 1992.
- [5] Thomas R H, Kinzie K W and Pao S P. Computational analysis of a pylon-chevron core nozzle interaction. *7th AIAA/CEAS Aeroacoustics Conference*, AIAA Paper No. 2001-2185, 2001.
- [6] Engblom W A, Khavaran A and Bridges J. Investigation of variable-diffusion turbulence model correction for round jets. *11th AIAA/CEAS Aeroacoustics Conference*, AIAA Paper No. 2005-3085, 2005.
- [7] Thies A T and Tam C K W. computation of turbulent axisymmetric and nonaxisymmetric jet flows using the k- $\epsilon$  model. *AIAA Journal*, Vol. 34, No. 2, pp 309-316, 1996.
- [8] Tam C K W and Ganesan A. k- $\epsilon$  turbulence model for calculating hot jet mean flows and noise. *AIAA Journal*, Vol. 42, No. 1, pp 26-34, 2004.
- [9] Abdol-Hamid K S, Pao S P, Massey S J and Elmiligui A. Temperature corrected turbulence model for high temperature jet flow. *Journal of Fluids Engineering*, Vol.126, pp 844-850, 2004.
- [10] Jones W P and Launder B E. The prediction of laminarization with a two-equation model of turbulence. *International Journal of Heat and Mass Transfer*, Vol. 15, No. 2, pp 301-314, 1972.
- [11] Menter F R, Kuntz M and Langtry R. Ten years of industrial experience with the SST turbulence model. *Heat and Mass Transfer*, Vol. 4, 2003.
- [12] Wilcox D C. Reassessment of the scale-determining equation for advanced turbulence models *AIAA Journal*, Vol. 26, No. 11, pp 1299-1310, 1972.
- [13] Menter F R. Zonal two equation k-omega turbulence models for aerodynamic flows. *24th Fluid Dynamics Conference*, AIAA Paper No. 93-2906, 1993.
- [14] Menter F R. Two-equation eddy-viscosity turbulence models for engineering applications. *AIAA Journal*, Vol. 32, No. 8, pp 269-289, 1994.
- [15] Sarkar S, Erlebacher G, Hussaini M Y and Kreiss H O. The analysis and modeling of dilatational terms in compressible turbulence. *Journal of Fluid Mechanics*, Vol. 227, pp 473-495, 1991.
- [16] Suzen Y B and Hoffmann K A. Investigation of supersonic jet exhaust flow by one- and two-equation turbulence models. *36th Aerospace Sciences Meeting & Exhibit*, AIAA Paper No. 98-0322, 1998.
- [17] Wilcox D C. *Turbulence modeling for cfd*, 2nd ed., DCW Industries, 1998.
- [18] Saegeler S, Mundt Ch. Einfluss der Modellierung von Temperaturturbulenz auf die Mischung von Triebwerksstrahlen. *acc. for 61st DGLR Kongress*, Berlin, 2012.
- [19] Borm O, Jemcov A, Kau H-P. Density based navier stokes solver for transonic flows. *6th OpenFOAM Workshop*, PennState University, USA, 2011.
- [20] Saegeler S, Mundt Ch, Implementation of a preconditioner for a density-based navier-stokes solver. *acc. for 7th OpenFOAM Workshop*, Technische Universität Darmstadt, Germany, 2012.
- [21] Mattingly J D, Heiser W H and Pratt D T. *Aircraft engine design*, 2nd ed., American Institute of Aeronautics and Astronautics, Inc., 2002.
- [22] Bräunling W J G. *Flugzeugtriebwerke*, Springerverlag, 2001.